

Composite Pt/(SnO₂/C) and PtSnNi/C Catalysts for Oxygen Reduction and Alcohol Electrooxidation Reactions

D. K. Mauer^{a, *}, S. V. Belenov^a, L. M. Skibina^{a, †}, and V. E. Guterman^a

^a Southern Federal University, Rostov-on-Don, Russia

*e-mail: mauer@sfnu.ru

Received October 1, 2020; revised January 10, 2021; accepted January 21, 2021

Abstract—The electrodeposition of tin and tin-nickel on a highly dispersed carbon material is used to obtain composite supports. These composite supports were used in the Pt(0) nanoparticles deposition from Pt(IV) solution by chemical reduction. The composition, structure, and activity of the obtained Pt(SnO₂/C) and PtSnNi/C catalysts in the oxygen reduction and alcohol electrooxidation reactions were studied. The composite-support-based platinum catalysts exhibit higher activity in the reactions of alcohols electrooxidation in comparison with the commercial Pt/C analogue. Trimetallic PtSnNi/C catalysts are the most promising materials for the electrooxidation of alcohols.

Keywords: platinum-containing catalysts, nanoparticles, composite support, alloying of platinum, electrooxidation of alcohols

DOI: 10.1134/S1023193521060069

INTRODUCTION

The low-temperature fuel cell performance is based on electrochemical reactions of a reductant (e.g., hydrogen or methanol) oxidation and oxidant (O₂) reduction occurring at the catalyst's highly developed surface. The catalysts activity and stability depend on their composition and structure, above all [1].

The most effective catalysts for the low-temperature fuel cells are materials containing nanoparticles of platinum or its alloys with some *d*-metals, deposited onto carbonaceous or oxide support surfaces [2–6]. The platinum deposition in the form of nanosized particles increased the active surface area per the noble metal unit mass, although the nanoparticles aggregation and degradation processes gradually lower their catalytic activity [6, 7]. Considering the platinum nanoparticles distribution uniformity, their adhesion strength, and resistivity against degradation (leading to the nanoparticles agglomeration or falling off from the surface), the support role can hardly be overestimated. The ability of the platinum-containing catalysts composition and microstructure control is important for the keeping of their high activity and non-degradation property [8–12].

The extension of scope of the fuel cells raised problems connected with the requirements of keeping the electrocatalyst active, with the simultaneous decrease in the noble metal loading. A perspective trend is the support preparation of composite materials consisting

of metal oxides and carbon. It allowed obtaining corrosion-stable active catalysts superior to commercial Pt/C-catalysts [13, 14]. The materials advantages, as compared with carbon, are: the adhesion strengthening and the particles more uniform distribution over the support surface. As a consequence, the electrochemically active surface area increased, along with the catalytic activity in the alcohol oxidation and the platinum-containing catalyst stability [15].

The electrochemical deposition of metals from their salt solutions onto carbonaceous support is a simple and technological method of the metal oxide/carbon composite supports synthesis [16]. The method was developed on the basis of the earlier suggested method of the platinum nanoparticle formation at disperse carbonaceous support particles [17]. To prepare composite supports for platinum catalysts, it is meaningful using the methods of the oxide component applying to carbon which provide further possibility to supply/remove electrons to (from) the platinum nanoparticles. One more approach to the metal oxide/carbon composite supports is the metal electrode pulse electrochemical dispersing in a carbon suspension [18], where thus obtained metal particles are spontaneously oxidized to oxides; the latter then are deposited onto the carbonaceous support.

Of special interest is the SnO₂/C system possessing sufficient electronic conductivity. The SnO₂ crystal nanosized structure provided the oxide high specific surface area and affected properties and capacity of numerous materials and devices based on the using of

[†] Deceased.

this system: gas sensors, photodetectors, photocatalysts, antistatic coatings, dye-sensitizers, solar cells, etc. [19]. Different types of the SnO₂ particles and films can be prepared by pyrolysis [20, 21], laser ablation [22, 23], sol-gel procedure [24, 25], and homogeneous deposition [26, 27]. At that, the SnO₂-containing material morphology control still remains a complicated problem. The problem could be solved by the using of electrochemical methods for the nanodisperse SnO₂ preparation. It is known that catalysts based on the compositex SnO₂/C-supports demonstrate improved activity in the ethanol and methanol oxidation reactions. For example, the study of electrochemical behavior of the Pt/(SnO₂/C)-catalysts in comparison with their Pt/C-analogs revealed a decrease in the methanol/ethanol electrooxidation potential and the process simultaneous acceleration [18]. The synthesized Pt/(SnO₂/C)-catalyst [28] demonstrated excellent catalytic activity, long service life, and high tolerance to the methanol oxidation intermediate products as compared with the commercial Pt/C-material. In the authors' opinion, the elevated catalytic effectiveness is connected with the Pt-to-SnO₂ electronic interaction, as well as Pt (111) plane high fraction in the metal nanocrystals. It is believed that the electron effective transfer and the platinum nanoparticles stabilization is promoted by the nanoparticle interaction with SnO₂ and carbon [28]. The composite Pt/(SnO₂/C)-materials are also considered as catalysts in the ethanol oxidation reaction [29, 30]; their activity is comparable with the currently most effective PtRu/C-catalysts for the methanol and ethanol oxidation [31–33]. However, analysis of literature data allowed concluding that it is trimetallic platinum-containing materials that is the next step in the developing of catalysts for the ethanol oxidation [34–36]. In particular, synthesis and application of PtSnNi/C-catalysts for the ethanol oxidation reaction were described [34]. Moreover, it was reported [35] that it is right the PtSnNi/C-catalysts that are the most active in the ethanol oxidation reaction of all multicomponent systems, such as PtRuNi/C, PtSnRh/C, PtSn/C, and PtSnNi/C. It is to be noted that all materials in work [35] were synthesized in liquid phase by polyol method with the using of polyvinylpyrrolidone as stabilizer; the average size of metal crystallites in thus prepared catalysts was about 4 nm. In some works (e.g., [36]) the PtSnNi/C-catalysts with the summary metal mass fraction of 20% and the Pt : Sn : Ni mass ratio of 60 : 40 : 40 were deposited onto different supports: the Vulcan XC-72 carbon black and functionalized multiwall carbon nanotubes. The using of the Vulcan XC-72 as a support was shown [36] to allow obtaining higher electrochemical characteristics, yet, lower stability as compared with a Pt:Sn:Ni-catalyst deposited onto the carbon nanotubes. Along with this, ternary metal systems, the Pt–Sn–Ni in particular, deposited onto carbonaceous

supports, are still scarcely studied as catalysts in the oxygen reduction reaction (ORR) and that of alcohol oxidation. The study of mechanism of the alcohol oxidation at catalysts of different composition and search for the most effective materials for the methanol- and ethanol-based direct fuel cells are rather fast-growing trend nowadays [37, 38].

Thus, both the platinum alloying by some *d*-metals and the co-present platinum nanoparticles and tin oxide at the catalytic support surface can increase the catalyst activity, the more so, in the alcohol oxidation reactions. We believe that the SnO₂/C composite prepared by the tin pre-deposition with the metal nanoparticles subsequent spontaneous oxidation can appear as a perspective support for the platinum-containing electrocatalysts under the condition that the oxide has been formed as nanosized particles strongly attached to the disperse carbon surface. In the other extreme, we can see that the very possibility to combine the positive effect of the platinum-alloying component and the tin oxide nanoparticles in a single catalyst is still underexplored.

Having regard to the above, in this work we aimed at the preparing of nanostructured composite supports of the type “metal oxide/carbon” and their based two- and three-component platinum-containing catalysts, as well as studying of characteristics of the catalysts in the ORR, methanol oxidation, and ethanol oxidation reactions.

EXPERIMENTAL

To electrodeposit metals onto disperse carbonaceous support in its suspension, we used a glassy carbon anode with surface area of 19.5 cm² and copper cathode (1.5 cm²). Both were plunged into the suspension ultrasound-dispersed immediately prior to electrodeposition and containing 0.5 g of the Vulcan XC-72 carbonaceous powder in 50 mL of electrolyte. Tin was deposited from tinning-electrolyte described in [39] containing 0.25 M SnSO₄ and 0.1 M H₂SO₄. To simultaneously deposit tin and nickel, we used a mixed electrolyte also used for deposition of the SnNi-alloy onto stationary electrodes [40], containing 0.25 M SnCl₂, 0.25 M NiCl₂ and 0.14 M NH₄F. The electrodeposition was carried out at the room temperature under steady agitation, to keep the system uniform. Upon the preliminary studying of different current regimes of the metal electrodeposition, we choose two items: 9 A for 3.7 min and 1.6 A for 21 min.

Upon the metal(s) electrodeposition, the suspension was filtered off using a Buchner funnel (the blue-band filter), and washed with distilled water. The obtained support was dried on the filter for 4 h at a temperature of 80°C. In what follows, the materials prepared by the Sn and Sn–Ni deposition onto disperse carbonaceous support will be denoted SC and NSC, respectively.

To deposit platinum onto the SC and NSC composite supports, we used procedure of the boron-hydride synthesis [6]. A composite support (0.10–0.30 g) was placed to a mixture of ethylene glycol (30 mL) and twice distilled water (30 mL), then estimated amount of $\text{H}_2[\text{PtCl}_6] \cdot 6\text{H}_2\text{O}$ aqueous solution was added under agitation. The obtained suspension was homogenized by sonication for 5 min, after which the solution pH was made up to 11 by adding 0.1 M NaOH solution. Further, a three-fold excess of freshly prepared 0.5 M NaBH_4 aqueous solution was added under agitation. The suspension was allowed to stand for 40 min under agitation, then the obtained catalyst was separated by filtering with subsequent repeated washing with twice distilled water and ethanol. The samples were dried at the temperature of 80°C for 2 h.

The Pt : Ni : Sn metal mole ratio in the multicomponent catalysts was determined by X-ray fluorescence analysis using a RFS-001 spectrometer with full external reflection of X-ray radiation (Research Institute of physics, the Southern Federal University). The exposure was 300 s. The X-ray fluorescence spectra were recorded and processed by using the UniverS program (the Southern Federal University). To determine the metal summary amount (tin, nickel, and platinum) in the synthesized materials, we used thermal analysis method: in particular, we determined the mass of substances remaining in the crucible after the carbon complete oxidation as a result of 30-minute heating at 800°C in air (5–10 mg of each sample). When calculating the metal mass fraction, we took into consideration that the post-calcination residue in the crucible consisted of tin and nickel oxides and the platinum metal.

The sample phase analysis and the nanoparticle (crystallite) size were determined by the X-ray diffraction analysis. X-ray patterns were registered using an ARL X'TRA diffractometer with Bragg–Brentano geometry. Typical settings were: 40 kV, 35 mA, scan step 0.02 deg in the 2θ coordinates, scanning rate 2 deg/min. The phase analysis was based on the data from open access publications, in particular, the Crystallography Open Database (COD) [41, 42].

The X-ray patterns were analyzed using a SciDavIs software package; the peak location, their full width at the peak half maximum (FWHM), and area were determined on the basis of approximated Lorentz function. From the X-ray patterns, the platinum and the alloys crystallite average size was determined using (111) reflections; that of tin dioxide, using (101) reflections. The crystallite average size was determined using Scherrer formula (1) [43] upon the substituting the FWHM therein:

$$D_{hkl} = K\lambda / [\text{FWHM} \cos \theta], \quad (1)$$

where λ is the monochromatic radiation wavelength; FWHM is the full peak width at its half maximum (radian); D_{hkl} is the average thickness of the stack of

reflecting planes in the field of coherent dissipation, that is, the crystallite average diameter; θ is the reflection angle; $K = 0.89$ is the Scherrer constant. To allow for the instrumental broadening, the diffractometer was pre-calibrated using a standard, for which an annealed polycrystalline α -quartz plate was used, whose grains were sized 2 to 4 μm .

To determine the platinum electrochemically active surface area, we used cyclic voltammetry. A thin (about 4 μm) layer of the studied material was applied to end-face of a rotating disc electrode. To this purpose, 6 μL of the catalyst suspension in water–isopropanol mixture containing 0.6 μg of the catalyst, added with the Nafion polymer, was applied to the end-face of a glassy carbon rotating disc electrode. After drying, another 7 μL of 0.05% Nafion solution was added for the film fastening, after which the electrode was dried for 5 min at the room temperature. The potential scanning was done by a VersaSTAT 3 potentiostat (AMETEK Scientific Instruments, USA), which also recorded the current. Firstly, to standardize the platinum surface and remove contaminations entirely, its potential was cycled (100 cycles) with the potential scanning rate of 200 mV s^{-1} over the potential range from 0.05 to 1.2 V (RHE). Then, two cyclic voltammograms were recorded over the 0.05–1.2 V range at a potential scanning rate of 20 mV s^{-1} . The passed charge was found by integration of the “hydrogen” segment of the cyclic voltammograms in the “current–time” coordinates using a VersaStudio software package. To this purpose, we averaged the charges consumed in the hydrogen electrochemical adsorption and desorption at platinum after subtraction of the charge consumed for the electrical double layer charging. All measurements were carried out at the room temperature. The electrochemically active surface area S was calculated by the following formula:

$$S = \frac{Q}{m \cdot 210}, \text{ cm}^2/\text{g}(\text{Pt}), \quad (2)$$

where Q is the average value (half-sum) of the charges (μC) consumed in the hydrogen electrochemical adsorption and desorption; m is the platinum mass at the electrode (g); 210 ($\mu\text{C}/\text{cm}^2$) is the charge required for the atomic hydrogen monolayer electrochemical adsorption and desorption per 1 cm^2 of the platinum surface.

To determine the metal active surface area from the amount of electrochemically oxidized chemisorbed CO, we bubbled CO through the electrolyte for 30 min, then argon for 30 min, by keeping constant the electrode potential at 0.1 V. Then, cyclic voltammograms (3 cycles) were recorded over the potential region from 0.05 to 1.20 V at a potential scanning rate of 20 mV s^{-1} . The electrochemically active surface area was calculated from the charge consumed in the oxidation of CO chemisorbed at the metal surface. To this purpose, we substituted 420 $\mu\text{C}/\text{cm}^2$ to the formula (2)

Table 1. Characteristics of materials obtained by the Sn electrodeposition (SC) and Ni and Sn co-deposition (NSC) onto carbonaceous support Vulcan XC-72

Sample	The samples phase composition according to X-ray diffraction analysis	Mass fraction of metals, wt %	Metal component composition (X-ray fluorescent analysis)	The Ni(SnOH) ₆ crystallite average size, nm	The SnO ₂ crystallite average size, nm
SC-1	SnO ₂ , Sn	16 ± 1.5	Sn	—	2.7 ± 0.2
SC-2	SnO ₂ , Sn	35 ± 3.5	Sn	—	1.8 ± 0.2
NSC-1	Ni(SnOH) ₆ , Ni, NiO	14 ± 1.5	Ni _{3,7} Sn	60 ± 5	—
NSC-2	Ni(SnOH) ₆ , Ni, NiO	32 ± 3.5	Ni _{4,7} Sn	150 ± 5	—

for 210 μC/cm², because the charge consumed in the oxidation of 1 mole of CO is twice as large compared to that consumed in the oxidation of 1 mole of H_{ad}.

After the determination of the materials electrochemically active surface area, we studied their activity in the ORR at the disc electrode rotation velocities of 400, 900, 1600, and 2500 rpm. Preliminarily, linear-sweep-potential voltammograms were recorded in argon atmosphere, to be subtracted from those recorded in the oxygen atmosphere: $I = I_{O_2} - I_{Ar}$. In this way, the background currents were allowed for. The measurements were carried out in a standard three-electrode cell, with the using of 0.1 M HClO₄ solution as indifferent electrolyte. Prior to the measurements, the working solution was bubbled-through with O₂ for 40 min under atmospheric pressure. The voltammograms were taken starting at 0.02 V and up to 1.20 V with the potential scanning rate of 20 mV s⁻¹. Further, the dependence of the current on the disc electrode rotation velocity was analyzed by using the Koutecky–Levich equation. The measurements results were corrected for the system Ohmic resistance ($R = 26$ Ohm), as described elsewhere [44].

When measuring the catalysts activity in the methanol or ethanol oxidation reactions, solutions 0.1 M HClO₄ + 0.5 M methanol/ethanol were the working electrolyte. The charge consumed in the alcohol oxidation in a single potential cycle was calculated by an oxidation current peak in the potential direct scan. Chronoamperograms were taken at a potential of 0.6 V. All these measurements were carried out at a stationary disc electrode in argon atmosphere.

Because the absolute values of the electrochemically active surface area and catalyst activity in electrochemical reactions are very sensitive to the catalytic layer structure and electrolyte purity, we used commercial Pt/C-catalyst HiSPEC3000 (Johnson Matthey) containing 20 wt % Pt as a standard sample. When studying the prepared catalyst activity in the alcohol oxidation reactions, we also used a commercial PtRu/C-electrocatalyst (Pt : Ru 1 : 1, 40 wt % Pt, 20 wt % Ru, Alfa Aesar) as a reference. The catalytic ink composition and the HiSPEC3000 and PtRu/C

catalytic layer deposition procedure were the same as for the studied catalysts.

Silver-chloride electrode was the reference electrode. All potential values in the paper are given against reversible hydrogen electrode (RHE).

RESULTS AND DISCUSSION

Synthesis and Structure of the SC and NSC Composite Supports and Platinum-Containing Catalysts on Their Basis

By using two different current modes (see Experimental section), we obtained materials containing about 15% of the metals (SC-1 and NSC-1 obtained with the current of 9 A) or about 35% of the metals (SC-2 and NSC-2 obtained with the current of 1.6 A) (Table 1). The metal deposition onto the carbonaceous support was confirmed by thermogravimetry; the elemental investigation of the obtained materials by the X-ray fluorescent analysis confirmed the presence of both tin and nickel atoms in the NSC series catalysts (Table 1). At that, with the increasing of the metal mass fraction the nickel fraction in the NSC series samples changed upward.

To determine the sample phase composition and the crystallite size, the obtained materials were studied by using X-ray diffraction analysis. The X-ray patterns of the sample obtained by the tin deposition onto carbonaceous support shows reflections of two phases: SnO₂ and Sn (Fig. 1, curve 1). The reflections corresponding to the tin oxide phase are strongly broadened. The SnO₂ crystallite average size calculated by the Scherrer formula for the SC-1 and SC-2 materials is about 2.7 and 1.8 nm, respectively (Table 2). The reflections in the X-ray patterns corresponding to the tin metal phase are characterized by smaller broadening as compared with those of the SnO₂ phase; hence, the crystallite average size cannot be determined with fair accuracy here.

The X-ray patterns of the NSC composite materials obtained in the electrolyte containing tin and nickel chlorides show well pronounced peaks that can be ascribed to NiSn(OH)₆, NiO, and Ni phases (Fig. 1,

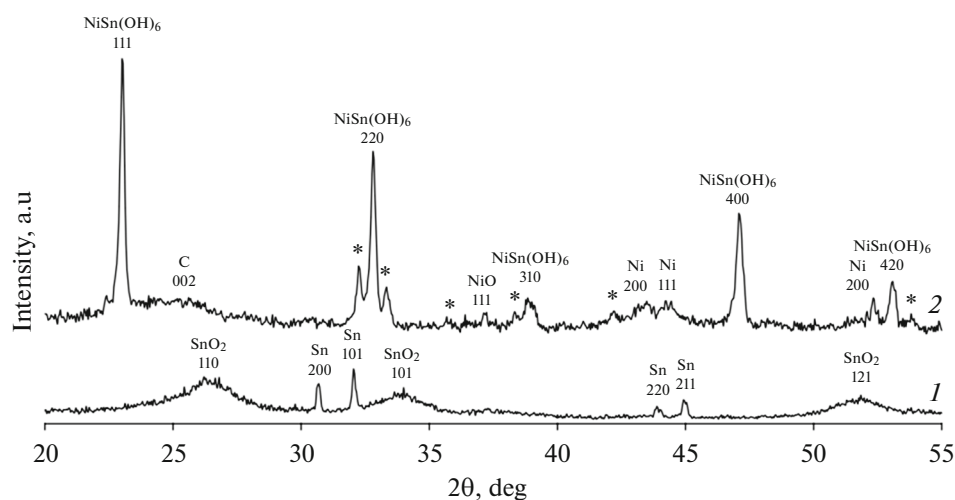


Fig. 1. X-ray diffraction patterns of the materials: (1) SC-2, (2) NSC-2.

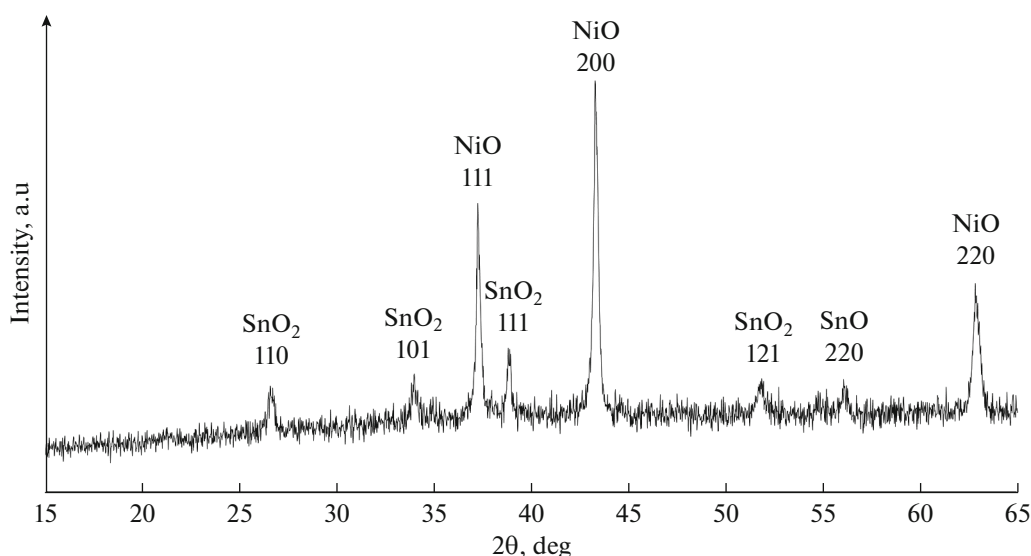


Fig. 2. X-ray diffraction patterns of the NSC-2 material's residue after high-temperature oxidation.

curve 2). Extra reflections denoted with asterisks (*) in the X-ray patterns can be linked to $\text{NiSnO}_3 \cdot x\text{H}_2\text{O}$ phases with non-permanent composition. At that, no reflections corresponding to the Sn or SnO_2 phases were detected in the X-ray patterns of the NSC-2 material.

For the NSC-2 material, from the full width at the peak half maximum (FWHM) we calculated the NiSn(OH)_6 phase average crystallite size: about 150 nm (Table 1). No calculations of the average crystallite size were carried out for the reflections corresponding to the NiO and Ni phases because of their low intensity. The X-ray diffraction analysis was also used in the studying of oxidation products formed after long exposure of samples to 800°C in air. X-ray patterns of a residue obtained by the NSC-2 material sintering

(Fig. 2) show reflections of two phases, SnO_2 and NiO, which is in good agreement with the data on the initial composition of these materials “as prepared.”

Thus, by using metal electrodeposition onto Vulcan XC-72 carbonaceous material we obtained composite supports that contained, in the case of the SC series samples, SnO_2 nanoparticles and tin metal in addition to highly disperse carbon; in the case of the NSC series samples, particles of nickel metal, nickel oxide, and rather coarse NiSn(OH)_6 phase particles.

To prepare platinum-containing catalysts on the basis of the obtained SC and NSC composite supports, we deposited platinum onto the composite materials by chemical reduction. We controlled the amount of platinum precursor (H_2PtCl_6) in order to

Table 2. Continuous and structural characteristics of the PSC- and PNSC-catalyst samples and the Pt/C commercial material

Sample	Mass fraction of Pt, $\omega(\text{Pt})$, %	The component ratio (X-ray fluorescent analysis)	The PtNi _x Composition after electrochemical measurements (X-ray fluorescent analysis)	The SnO ₂ crystallite average size, nm	The Pt crystallite average size, nm
PSC-1	17	PtSn _{1.5}	—	2.7 ± 0.2	3.3 ± 0.2
PSC-2	19	PtSn _{1.7}	—	1.8 ± 0.2	3.8 ± 0.2
PNSC-1	21	PtNi _{1.0} Sn _{0.32} (Pt _{3.1} Ni _{3.1} Sn)	PtNi _{0.29}	—	3.9 ± 0.2
PNSC-2	23	PtNi _{1.2} Sn _{0.25} (Pt ₄ Ni _{4.8} Sn)	PtNi _{0.45}	—	2.2 ± 0.2
JM20	20	Pt	Pt	—	2.2 ± 0.2
PtRu	40	Pt ₁ Ru ₁	—	—	3.2 ± 0.2

obtain materials with the platinum content of 20 wt %. The obtained samples were denoted PSC and PNSC. The platinum content in the materials was determined from the data of thermogravimetric measurements, with due allowance for the corresponding oxide formation and the results of the X-ray fluorescent analysis of the samples (Table 2). It came to 17–23 wt %, which approached the calculated figure (20 wt %). It is to be noted that the higher relative nickel content in the NSC-2 material, as compared with the NSC-1 one, was retained after the platinum deposition thereon as well (Table 2).

The X-ray diffraction patterns of the PSC-1 and PSC-2 samples obtained after the platinum deposition onto the SC series materials show reflections of the platinum and SnO₂ phases (Fig. 3, curves 1, 2). The platinum particles average size in the materials came to 3.3 and 3.8 nm (Table 2). When comparing the X-ray diffraction patterns of the SC-2 (Fig. 1, curve 1) and PSC-2 (Fig. 3, curve 2) samples, we see that the SnO₂ phase reflections obtained prior to and after platinum deposition remained practically unchanged; no tin metal reflections is observed after the platinum deposition. In all probability, the tin metal phase present in the SC series materials in small amounts, was dissolved after the hexachloroplatinic acid adding in the course of the synthesis.

The maximums in the X-ray diffraction patterns of the commercial PtRu/C-catalyst are shifted toward larger 2 θ angles as compared with the Pt/C-material, which is characteristic of the Pt–Ru solid solution.

The special feature of the X-ray diffraction patterns of the PNSC-materials (Fig. 3, curves 3, 4) obtained with the involving of the NSC-supports (Fig. 1, curve 2) is the absence of reflections corresponding to the Ni(SnOH)₆, Ni, and NiO phases. This can be

explained by the Ni(SnOH)₆, Ni, and NiO dissolution in acidic medium (on the adding of H₂PtCl₆) and subsequent partial co-deposition of the dissolved metals together with platinum during their interaction with reductant in the course of the synthesis. Indeed, the X-ray diffraction patterns of the PNSC-samples show significant shift of the maximums of the platinum reflections toward larger 2 θ angles as compared with the Pt phase: from 39.7 to 41 deg, which points to the formation of a PtNi or PtSnNi solid solution. The formation of the platinum-based disordered solid solution with cubic face-centered crystal lattice lead to decrease in the lattice parameter of nanoparticles in the PNSC-1 (3.859 Å) and PNSC-2 (3.838 Å) samples as compared with pure platinum (3.923 Å).

It is known [45, 46] that the adding of tin atoms to the platinum-based solid solution leads to increase in the crystal lattice parameter; it also shifts the maximums of reflections in X-ray diffraction patterns toward lesser 2 θ angles as compared with that of pure platinum, while the alloying of platinum with nickel demonstrates the opposite trend [47]. For example, in work [48] the PtSnNi/C-materials (Pt₇₅Sn₁₅Ni₁₀ and Pt₅₅Sn₁₇Ni₂₈) had the lattice parameters 3.923 and 3.913 Å, respectively, which is close to that of pure platinum. This was explained right by the differently directed effects of the alloying by the nickel and tin atoms. Similar effect of the platinum alloying with the nickel and tin atoms was observed for Pt₈₀Sn₁₀Ni₁₀-material with the lattice parameter 3.906 Å [49].

In the obtained PNSC-1 and PNSC-2 materials, the Ni atomic fraction exceeds that of Sn by a factor of 3.1 and 4.8, respectively (Table 2). The data on the materials composition is in good agreement with the crystal lattice parameter: for the PNSC-2 sample containing larger nickel fraction, the crystal lattice param-

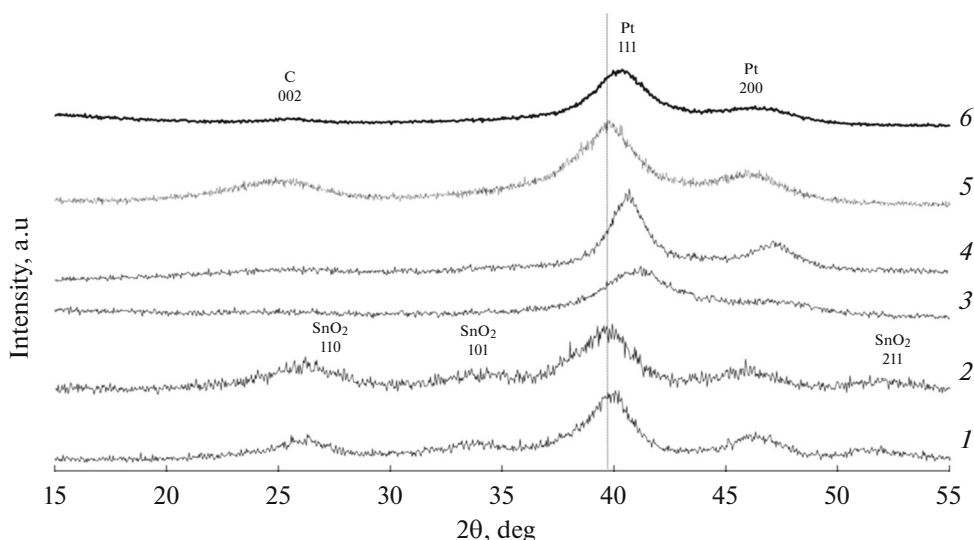


Fig. 3. X-ray diffraction patterns of the PSC and PNSC materials: (1) PSC-1; (2) PSC-2; (3) PNSC-1; (4) PNSC-2; (5) commercial Pt/C sample (JM20); (6) commercial PtRu/C sample.

eter (3.838 Å) is less than that of the PNSC-1 sample (3.859 Å). This fact is important in terms of the catalyst activity forecasting because results of works [50, 51] pointed to positive effect of the nickel atom high concentration in Pt–Ni solid solution on the catalyst activity in the ORR, which is due to decrease of the alloy crystal lattice parameter as compared with Pt.

Our calculations showed that the platinum crystallite average size in the PNSC-2 material (2.2 nm) is much less than that in the PNSC-1 (3.9 nm). We note that the average size of the platinum-based solid solution crystallites in the PNSC-2 material is close to those in the commercial Pt/C-catalyst (Table 2) and PtSnNi/C-catalyst obtained in work [49]. At the same time, it is significantly less than the crystallite size in the PtSnNi materials obtained in works [36] (5.14 nm) and [48] (3.8 nm).

To complete the discussion of the X-ray diffraction, we note that the estimating of the PNSC-1 and PNSC-2 material composition by using Vegard's law (linear dependence of the lattice parameter on the content of alloying constituent in solid solution) [52, 53] on the basis of assumption that only nickel atoms are included to the solid solution gives the compositions PtNi_{0.18} and PtNi_{0.26}, which contradicts the result of the elemental analysis (Table 2). This may be due to the formation of three-component alloy PtNiSn, the solid solution nonuniformity, or the nickel atom incomplete building-in to the solid solution composition. It is also not inconceivable that X-ray amorphous tin and nickel oxides are present in the PNSC series material. Unfortunately, in this case the X-ray diffraction analysis cannot interpret the composition of the obtained platinum-based solid solutions unambiguously.

The Study of Activity of the Platinum-Containing Catalysts Prepared on the Basis of the SC and NSC Composite Supports

The appearance of cyclic voltammograms of standardized electrodes (Fig. 4) are typical of platinum-containing electrocatalysts, they include the region of hydrogen adsorption–desorption, the “electrical double layer,” and “oxygen” ones. In the hydrogen adsorption–desorption region, the specific current at the PSC- and PNSC-materials is less than that at the commercial Pt/C-catalyst. The latter has the largest electrochemically active surface area, while the electrochemically active surface area of our catalysts is less by 13–36% (Table 3). This fact may be caused either by larger size of crystallites in the prepared materials, or by more intensive nanoparticles agglomeration, e.g., in the PNCS-2 material. The determination of the electrochemically active surface area by the oxidation of the chemisorbed CO monolayer (Fig. 4b) gave close values of the electrochemically active surface area [45–48 m²/g (Pt)] for the three materials (PSC-1, PSC-2, and PNSC-1) and a higher value [63 m²/g (Pt)] for the PNSC-2 (Table 3) whose crystallites have lesser size (Table 2). Note that the electrochemically active surface area of the PtRu-catalyst [97 m²/g (Pt)] was determined only by the CO oxidation method because the applying of the hydrogen adsorption–desorption method to platinum–ruthenium catalysts is not quite correct [32]. By analyzing the CO oxidation peak positions in cyclic voltammograms, we obtained some extra information on the studied catalysts properties. The potentials of the CO oxidation onset and maximum for the PtRu-catalyst are significantly lower than those for the Pt/C-catalyst (Fig. 4b), which evidences some facilitation of the CO

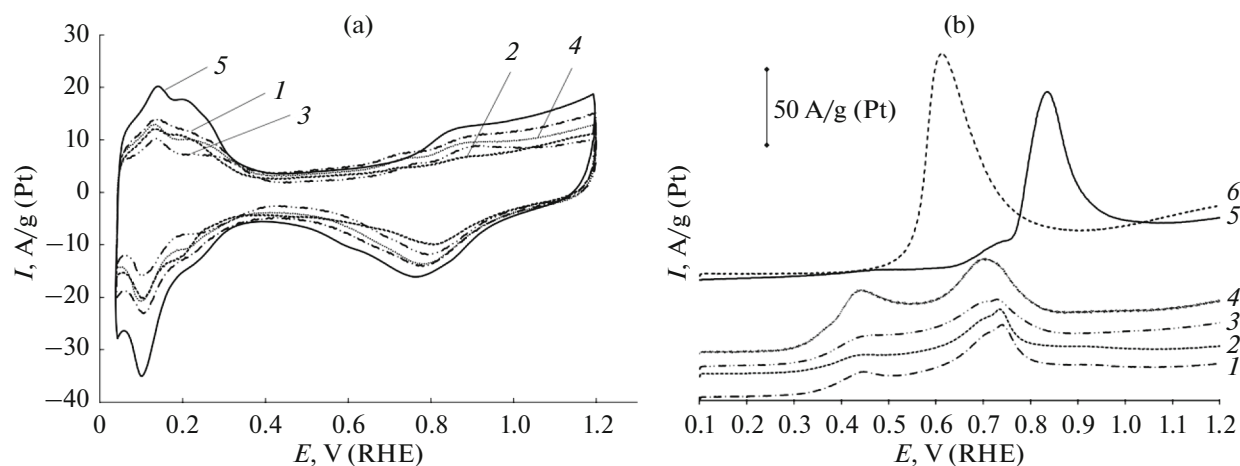


Fig. 4. Cyclic voltammograms (2nd cycle) (a) and fragments of cyclic voltammograms including peaks of the CO electrochemical desorption from the studied catalyst nanoparticles surface (b). Electrolyte: 1 M HClO₄, argon atmosphere. Potential scanning rate 40 mV s⁻¹: (1) PSC-1; (2) PSC-2; (3) PNSC-1; (4) PNSC-2; (5) commercial Pt/C sample (JM20); (6) commercial PtRu/C sample.

oxidation at the PtRu nanoparticles surface [37, 54]. Voltammograms of all PSC- and PNSC-materials show broad peak of the CO oxidation with two more or less pronounced maximums over the 0.44–0.45 V and 0.74–0.75 V potential ranges. The wide potential range of CO oxidation and the presence of two maximums can be connected with the nonuniformity of composition and structure of the multicomponent catalysts containing nanoparticles distinguishing significantly in their activity in the CO electrooxidation reaction. Note that the CO oxidation at potentials near 0.45 V occurring at the catalysts prepared in this work can evidence high activity in the alcohol oxidation reactions [55].

The estimate of composition of the PNSC-series materials after the voltammetric measurements (the Pt : Ni ratio about 3 : 1) showed the nickel partial dissolution in the sample (Table 2) down to the composition stabilization at the lower Pt : Ni mole ratio equal approximately to 3 : 1. Unfortunately, the determination of Sn content in the samples after the completing of the voltammetric measurements does not seem pos-

sible because of the small amount of the catalyst deposited onto the disc electrode end-face.

The PNSC series materials demonstrated the largest specific activity in the ORR per unit surface area: 2.7–2.8 A/m² (Pt). This may be due to the positive effect of the alloying on the platinum activity. Unfortunately, the lesser electrochemically active surface area of the PNSC-materials as compared with that of the commercial Pt/C-catalyst levels up this effect when the catalyst mass-activity is compared: at the potential of 0.90 V the mass-activity approached that of the PNSC-1, PNSC-2, JM20 samples (Table 3, Fig. 5): it came to 162–179 A/g (Pt). The samples prepared on the basis of the SC composite support demonstrated lower mass-activity in the ORR: 64–69 A/g (Pt). The number of electrons (n) involved in the current-generating reaction falls into the 3.8–4.1 range for all studied catalysts (Table 3). This evidently points to the predominant behavior of the oxygen electrooxidation reaction according to the four-electron mechanism.

Table 3. Some parameters characterizing electrochemical behavior of PSC-, PNSC-, and commercial Pt/C-catalysts

Sample	Electrochemically active surface area		Mass-activity, A/g (Pt) ($E = 0.90$ V)	Specific activity, A/m ² (Pt) ($E = 0.90$ V)	$E_{1/2}$ (ORR), V (1600 rpm)	Number of electrons in ORR at $E = 0.90$ V
	$H_{\text{ads/des}}$ m ² /g (Pt)	CO m ² /g (Pt)				
PSC-1	52 ± 5	45 ± 5	69 ± 3	1.3 ± 0.1	0.89	4.0
PSC-2	56 ± 5	48 ± 5	64 ± 3	1.6 ± 0.1	0.87	3.8
PNSC-1	58 ± 6	45 ± 5	162 ± 8	2.7 ± 0.1	0.92	3.9
PNSC-2	63 ± 6	63 ± 6	179 ± 9	2.8 ± 0.1	0.92	4.1
JM20	79 ± 8	78 ± 8	178 ± 9	2.2 ± 0.1	0.91	4.1

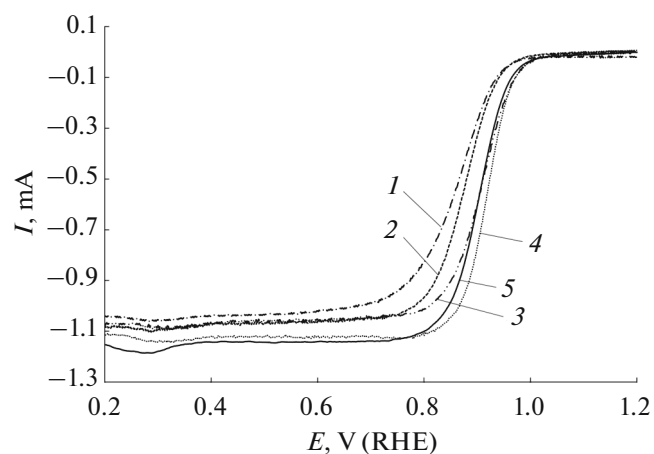


Fig. 5. Dependence of the oxygen electroreduction rate on the electrode potential. Catalysts: (1) PSC-1; (2) PSC-2; (3) PNSC-1; (4) PNSC-2; (5) commercial Pt/C sample (JM20)). Potential scanning rate 20 mV s^{-1} , disc rotation velocity 1600 rpm. 0.1 M HClO_4 , O_2 atmosphere.

To our knowledge, no information on the Pt–Ni–Sn-materials catalytic activity in the ORR can be found in literature; therefore, a correlation with literature data was traced only for the Pt/(SnO_2/C)-materials. In work [39], a Pt/(SnO_2/C)-catalyst showed higher half-wave potential and mass-activity (0.90 V and 153 A/g , respectively) as compared with parameters of analogous catalysts of the PSC-series, that were obtained in this work. At the same time, the support described in work [39] contained much less SnO_2 , whereas the platinum nanoparticles were deposited thereon with a synthesis procedure that differed from that we used in this work. In work [56], composite Pt/ SnO_2 -systems deposited onto carbon nanotubes and carbon paper were studied. Despite the fact of positive effect of the SnO_2 additive on the composite catalyst activity observed in work [56], the prepared materials had rather low activity in the ORR; on this reason, there's nothing to do except comparing their activity at the potential 0.85 V . In work [57], a num-

ber of catalysts were prepared at different oxide supports; among them, the largest specific activity [1.43 A/m^2 (Pt) at 0.90 V] was demonstrated by a Pt/ SnO_2/C -material. The above value approximately corresponds to the activity of the PSC-materials obtained in this work (Table 3).

To compare the platinum-containing catalysts activities in the alcohol oxidation reactions basing on the cyclic voltammetry data, few parameters must be used: the oxidation onset potential (E_o) [15, 34, 35, 46], the oxidation specific maximal current (I_{max}) in the direct potential scanning run [34, 45, 48, 58], and the charge consumed in the alcohol oxidation (Q), which can be determined by the peak in the voltammogram direct run [59]. Judging by the charge ($Q_{\text{CH}_3\text{OH}}$), consumed in the methanol oxidation in the direct potential scanning run (Table 4) and the methanol oxidation maximal current (I_{max}) (Fig. 6a), the studied catalysts can be ranked according to their activity: PtRu/C < PSC-1 < PSC-2 < PNSC-2 \leq PNSC-1. The result correlates well with the data [58] showing that the PtNiSn/C-catalyst activity, judging by the methanol oxidation maximal current, is by a factor of 1.8 larger than that of PtSn/C; by a factor of 1.24, than that of PtNi/C-materials. At the same time, the PtRu/C-catalyst demonstrated the lowest potential (E_o) of onset of the methanol oxidation, hence, the largest activity at relatively low potentials. To our view, it would make sense to compare the catalyst activity in the alcohol oxidation reactions by using chronoamperometry method at potentials approaching that of onset of the methanol oxidation (here 0.60 V). The methanol oxidation current in the initial stage of the measurements (I_{ini}) for the PNSC series materials is somewhat larger (Table 4, Fig. 6b) than that with PtRu/C-catalyst; much lower, with that from the PSC series. All studied samples showed significant decrease in the methanol oxidation current in the course of the chronoamperogram recording process (30 min); however, the largest current at the end of the measurements (I_{fin}) was also shown by the PNSC and PtRu/C-catalysts (Fig. 6b, Table 4). Thus, on the strength of all parameters, the

Table 4. Some parameters characterizing the catalysts electrochemical behavior in the alcohol oxidation reactions

Sample	Methanol					Ethanol				
	E_o , V	I_{max} , A/g (Pt)	$Q_{\text{CH}_3\text{OH}} \times 10^2$, C/g (Pt)	$I_{\text{CH}_3\text{OH}}$, A/g (Pt)		E_o , V	I_{max} , A/g (Pt)	$Q_{\text{C}_2\text{H}_5\text{OH}} \times 10^2$, C/g (Pt)	$I_{\text{C}_2\text{H}_5\text{OH}}$, A/g (Pt)	
				I_{ini}	I_{fin}				I_{ini}	I_{fin}
PSC-1	0.58	554 ± 28	46 ± 2	40 ± 2	13 ± 0.6	0.58	575 ± 29	139 ± 7	168 ± 8	47 ± 2
PSC-2	0.55	739 ± 37	73 ± 4	30 ± 1	10 ± 0.5	0.58	515 ± 26	137 ± 7	166 ± 8	44 ± 2
PNSC-1	0.54	958 ± 48	105 ± 5	107 ± 5	47 ± 2.3	0.29	848 ± 42	199 ± 10	281 ± 14	55 ± 3
PNSC-2	0.56	864 ± 43	94 ± 5	91 ± 5	51 ± 2.6	0.31	923 ± 46	259 ± 13	244 ± 12	66 ± 3
PtRu/C	0.47	376 ± 19	41 ± 2	89 ± 4	48 ± 2.4	0.58	508 ± 25	204 ± 10	136 ± 7	44 ± 2

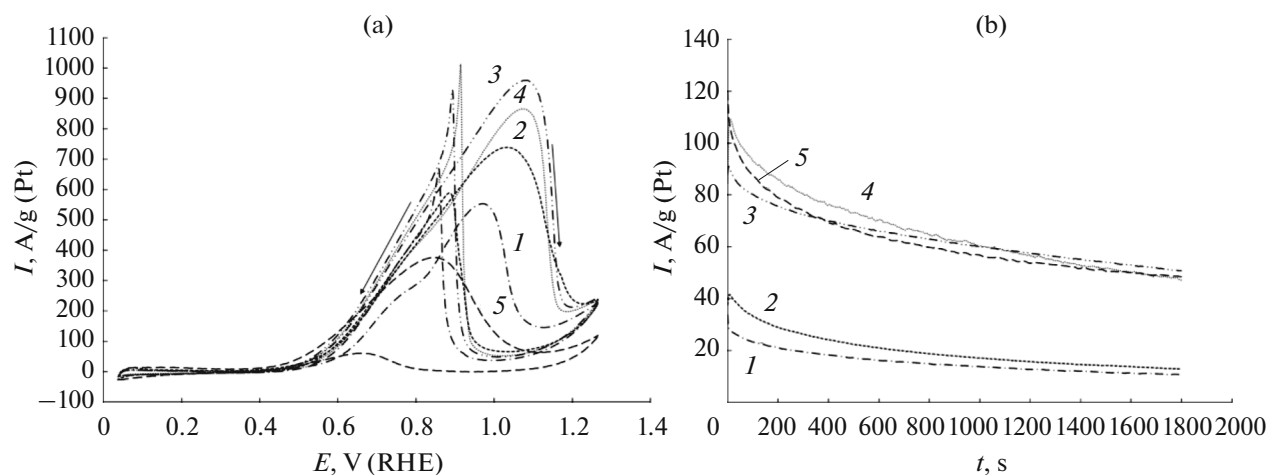


Fig. 6. Cyclic voltammograms (a) and chronoamperogram at potential 0.6 V (b) for: (1) PSC-1; (2) PSC-2; (3) PNSC-1; (4) PNSC-2; (5) commercial PtRu/C sample. Currents are normalized to the Pt mass. Electrolyte: 0.1 M HClO₄ solution added with 0.5 M CH₃OH, Ar atmosphere.

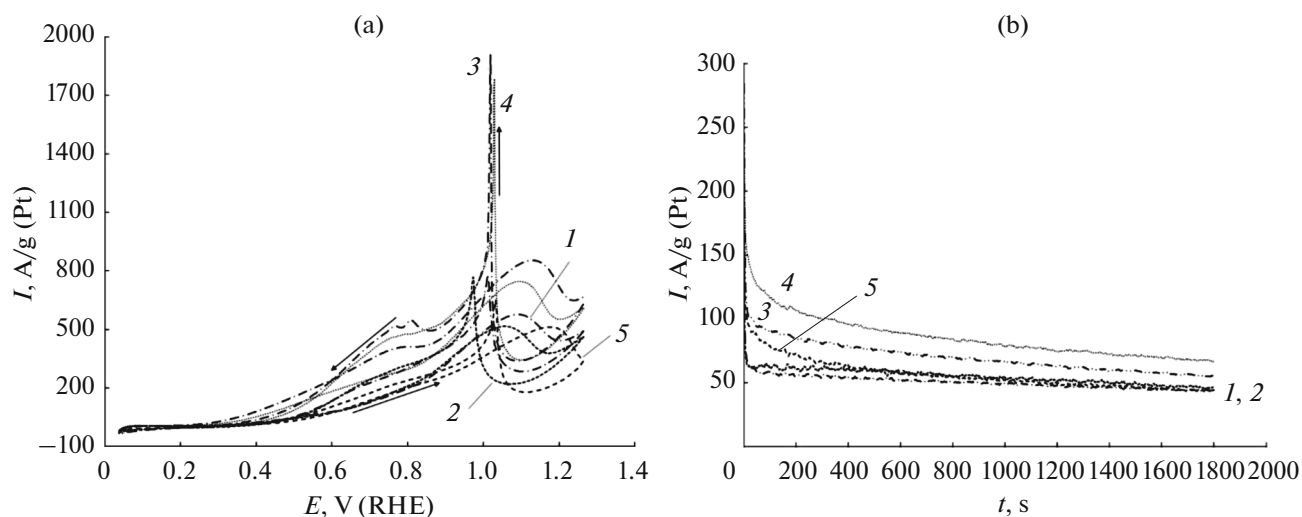


Fig. 7. Cyclic voltammograms (a) and chronoamperogram at potential 0.6 V (b) for: (1) PSC-1; (2) PSC-2; (3) PNSC-1; (4) PNSC-2; (5) commercial PtRu/C sample. Currents are normalized to the Pt mass. Electrolyte: 0.1 M HClO₄ solution added with 0.5 M C₂H₅OH, Ar atmosphere.

mass-activity of the obtained PtSnNi/C-materials in the methanol oxidation somewhat exceeds the activity of the commercial PtRu/C-catalyst.

On the comparing of electrochemical behavior of the studied materials in the ethanol oxidation, according to the cyclic voltammetry data, the most significant difference is observed in the ethanol oxidation onset potentials (E_0) (Fig. 7a, Table 4). For the three-metallic PtSnNi/C-materials of the PNSC series, the E_0 values are by approximately 0.30 V less as compared with the PSC- and PtRu/C-catalysts. On the comparing of the charge consumed in the ethanol oxidation during the direct run of the potential scanning ($Q_{C_2H_5OH}$), and the ethanol oxidation maximal current

(I_{max}) (Table 4, Fig. 7a), the PNSC series catalysts demonstrated the highest mass-activity in the ethanol oxidation. Thus, the studied materials can be ranked in the following series as regard their catalytic activity in the ethanol oxidation: PSC-2 \leq PSC-1 \leq PtRu/C $<$ PNSC-1 \leq PNSC-2. This series somewhat differs from the catalyst activity series in the methanol oxidation. The difference can be due to the difference in the methanol and ethanol oxidation mechanisms, in particular, with the possible involvement of the -C-C-bond disruption in the case of ethanol oxidation.

According to results of chronoamperometry, the three-metallic PtSnNi/C-materials demonstrate larger activity judging both by the initial current values and the current upon 30-min exposure to the potential

of 0.6 V (Fig. 7b, Table 4). Note that the commercial PtRu/C-catalyst is the least active with respect to the ethanol oxidation.

Thus, the three-metallic PtSnNi/C-materials demonstrate the largest catalytic activity with respect to the ethanol oxidation when judging by the data of both cyclic voltammetry and chronoamperometry at $E = 0.6$ V. The conclusion is in good agreement with the results of work [49] in which the Pt₈₀Sn₁₀Ni₁₀/C-catalyst showed the lowest onset potential in the ethanol oxidation and the highest catalytic activity over the entire potential range as compared to Pt₉₀Sn₁₀/C-, Pt₉₀Ni₁₀/C-, and Pt/C-materials. The Pt₈₀Sn₁₀Ni₁₀/C superiority was also confirmed [49] by the results of the catalyst testing in MEAs: the Pt₈₀Sn₁₀Ni₁₀/C-catalyst allowed reaching the maximal power exceeding those of the Pt₉₀Sn₁₀/C- and Pt/C-catalysts by a factor of 3.9 and 7.8, respectively. The PtSnNi/C-material obtained in work [48] also demonstrated higher activity in the ethanol oxidation as compared with Pt/C. The PtSnNi/C-catalyst improved activity in the ethanol oxidation can be caused by the facilitation of disruption of the C–C bond in the ethanol molecule at the nickel-alloyed platinum surface [49], as well as presence of tin dioxide nanoparticles which easily adsorb hydroxyl groups, and this facilitated the CO adsorbed molecule oxidation at lower potentials.

CONCLUSIONS

Composite supports of complicated composition containing tin and nickel (14 to 35%) were prepared by the Sn electrodeposition and Sn and Ni co-deposition onto highly disperse Vulcan XC-72 carbonaceous material. On the basis of the obtained composite supports, a series of catalysts was synthesized by using chemical reduction of platinum in liquid phase. The catalysts contained about 20 wt % Pt; the crystallite average size was 2.2 to 3.8 nm. Unlike the X-ray diffraction patterns of the supports, those of platinum-containing PSC and PNSC catalysts showed no reflections from Sn, Ni, NiO, and Ni(SnOH)₆ phases, which may be caused by the phases dissolution or transformation in the course of the platinum chemical deposition. The X-ray diffraction patterns of the PNSC-catalysts are characterized by a significant shift of the platinum reflection maximums toward larger 2θ angles as compared with the pure platinum phase, which evidences the formation of nanoparticles of the PtNi or PtSnNi solid solution in the course of the synthesis.

The mass-activity of the PNSC three-metallic materials in the ORR is shown approaching that of the commercial Pt/C-catalyst, despite their lower electrochemically active surface area; it exceeds the mass-activity of Pt(SnO₂/C)-materials significantly.

The behavior of the obtained PSC- and PNSC-catalysts in the alcohol oxidation reactions differs sig-

nificantly for methanol and ethanol, probably, because differences in the oxidation mechanisms of the alcohols. The commercial PtRu- and synthesized PtSnNi/C-catalysts of the PNSC series are more active in the methanol oxidation reaction than the Pt(SnO₂/C)-materials. At the same time, the PtRu/C-catalyst demonstrated the methanol oxidation onset potential by 70–90 mV less as compared with the three-metallic catalysts of the PNSC series. On the other hand, judging by all parameters, the prepared PtSnNi/C-catalysts are much more active in the ethanol oxidation than the commercial PtRu/C-catalyst.

The high activity of the ternary PtNiSn/C-catalysts in the alcohol oxidation reactions can be caused by the promoting effect of nickel additive on the platinum catalytic activity and the facilitating of hydroxyl group adsorption at the tin inclusions of tin oxide nanoparticles. Thus, the three-metallic catalysts are well perspective for the applications in alcohol-based fuel cells. Further studies of the materials composition and structure optimization are of significant interest.

ACKNOWLEDGMENTS

Authors acknowledged the assistance from A.Yu. Nikulin in the registration of X-ray patterns for the studied materials.

FUNDING

The reported study was funded by the Ministry of science and higher education RF under State contract no. 0852-2020-0019.

CONFLICT OF INTEREST

The authors declare that they have no conflict of interest.

REFERENCES

- Ioroi, T., Siroma, Z., Yamazaki, S., and Yasuda, K., Electrocatalysts for PEM Fuel Cells, *Advanced Energy Mater.*, 2018, vol. 9, no. 23, p. 1801284.
- Thompsett, D., *Catalysts for the Proton Exchange Membrane Fuel Cell*, Ed.: Vielstich, W., New York: Wiley, 2003, vol. 3, no. 6, p. 1.
- Zhang, J., Wang, X., Wu, C., Wang, H., Yiand, B., and Zhang, H., Preparation and characterization of Pt/C catalysts for PEMFC cathode: effect of different reduction methods, *React. Kinet. Catal. Lett.*, 2004, vol. 83, no. 2, p. 229.
- Chen, J., Jiang, C., Yang, X., Feng, L., B. Gallogly, E., and Wang, R., Studies on how to obtain the best catalytic activity of Pt/C catalyst by three reduction routes for methanol electrooxidation, *Electrochem. Commun.*, 2011, vol. 13, no. 4, p. 314.
- Prabhuram, J., Zhao, T.S., Wong, C.W., and Guo, J.W., Synthesis and physical/electrochemical characteriza-

- tion of Pt/C nanocatalyst for polymer electrolyte fuel cells, *J. Power Sources*, 2004, vol. 134, p. 1.
6. Guterman, V.E., Lastovina, T.A., Belenov, S.V., Tabachkova, N.Yu., Vlasenko, V.G., Khodos, I.I., and Balakshina, E.N., PtM/C (M = Ni, Cu, or Ag) electrocatalysts: Effects of alloying components on morphology and electrochemically active surface areas, *J. Solid State Electrochem.*, 2014, vol. 118, no. 5, p. 1307.
 7. Guterman, V.E., Belenov, S.V., Lastovina, T.A., Fokina, E.P., Prutsakova, N.V., and Konstantinova, Ya.B., Microstructure and electrochemically active surface area of PtM/C electrocatalysts, *Russ. J. Electrochem.*, 2011, vol. 47, p. 933.
 8. Petrii, O.A., Electrosynthesis of nanostructures and nanomaterials, *Uspekhi khimii*, 2015, vol. 84, p. 159.
 9. Yohannes, W., Belenov, S.V., Guterman, V.E., Skibina, L.M., Volotchaev, V.A., and Lyanguzov, N.V., Effect of ethylene glycol on electrochemical and morphological features of platinum electrodeposits from chloroplatinic acid, *J. Appl. Electrochem.*, 2015, vol. 45, p. 623.
 10. Leontyev, I.N., Kuriganova, A.B., Kudryavtsev, Y., Dkhil, B., and Smirnova, N.V., New life of a forgotten method: Electrochemical route toward highly efficient Pt/C catalysts for low-temperature fuel cells, *Appl. Catal. A*, 2012, vols. 431–432, p. 120.
 11. Moffat, T.P., Mallett, J.J., and Hwang, Sun-Mi., Oxygen Reduction Kinetics on Electrodeposited Pt, Pt_{100-x}Ni_x, and Pt_{100-x}Co_x, *J. Electrochem. Soc.*, 2009, vol. 156, p. 238.
 12. Gasteiger, H.A., Kocha, S.S., Sompalli, B., and Wagner, F.T., Progress in the synthesis of carbon nanotube- and nanofiber-supported Pt electrocatalysts for PEM fuel cell catalysis, *Appl. Catal. B: Environmental*, 2005, vol. 56, p. 9.
 13. Sharma, S. and Pollet, B.G., Support materials for PEMFC and DMFC electrocatalysts—A review, *J. Power Sources*, 2012, vol. 208, p. 96.
 14. Zhang, M., Yan, Z., Li, Y., Jing, J., and Xie, J., Preparation of cobalt silicide on graphene as Pt electrocatalyst supports for highly efficient and stable methanol oxidation in acidic media, *Electrochim. Acta*, 2015, vol. 161, p. 48.
 15. Zhao, R., Fu, G., Chen, Z., Tang, Y., Wang, Y., and Huang, S., Novel strategy for the synthesis of hollow Pt–Cu tetradecahedrons as an efficient electrocatalyst toward methanol oxidation, *Cryst. Eng. Comm.*, 2019, vol. 21, p. 1903.
 16. Guterman, V.E., Novomlinsky, I.N., Skibina, L.M., and Mauer, D.K., Russia Patent 2656914, 2018.
 17. Guterman, V.E., Novomlinsky, I.N., Alekseenko, A.A., Belenov, S.V., Tsvetkova, G.G., and Balakshina, E.N., Russia Patent 2616190, 2017.
 18. Kuriganova, A.B., Leontyeva, D.V., Ivanov, S., Bund, A., and Smirnova, N.V., Electrochemical dispersion technique for preparation of hybrid MO_x–C supports and Pt/MO_x–C electrocatalysts for low temperature fuel cells, *J. Appl. Electrochem.*, 2016, vol. 46, no. 12, p. 1245.
 19. Saha, M.S., Li, R., Cai, M., and Suna, X., High Electrolytic Activity of Platinum Nanoparticles on SnO₂ Nanowire-Based Electrodes, *Electrochem. Solid-State Lett.*, 2007, vol. 10, no. 8, p. 130.
 20. Lee, J.H. and Park, S.J.J., Nanoscaled oxide thin films for energy conversion, *Am. Ceram. Soc.*, 1993, vol. 76, p. 777.
 21. Williams, G. and Coles, G.S.V., Gas sensing properties of nanocrystalline metal oxide powders produced by a laser evaporation technique, *J. Mater. Chem.*, 1998, vol. 8, p. 1657.
 22. Willett, M.J., Burganos, V.N., Tsakiroglou, C.D., and Payatakes, A.C., Gas sensing and structural properties of variously pretreated nanopowder tin(IV) oxide samples, *Sens. Actuators B*, 1998, vol. 53, p. 76.
 23. Zhang, J. and Gao, L., Synthesis of SnO₂ Nanoparticles by the Sol–gel Method From Granulated Tin, *Chem. Lett.*, 2003, vol. 32, p. 458.
 24. De Monredon, S., Cellot, A., Ribot, F., Sanchez, C., Armelao, L., Gueneau, L., and Delattre, L., Synthesis and characterization of crystalline tin oxide nanoparticles, *J. Mater. Chem.*, 2002, vol. 12, p. 2396.
 25. Kumar, P., Khadtare, S., Park, J., and Yadav, B.C., Fabrication of leaf shaped SnO₂ nanoparticles via sol–gel route and its application for the optoelectronic humidity sensor, *Mater. Lett.*, 2020, vol. 278, p. 128451.
 26. Song, K.C. and Kang, Y., Preparation of high surface area tin oxide powders by a homogeneous precipitation method, *Mater. Lett.*, 2000, vol. 42, p. 283.
 27. Meiling, Dou, Ming, Hou, Dong, Liang, Wangting, Lu, Zhigang, Shao, and Baolian, Yi, SnO₂ nanocluster supported Pt catalyst with high stability for proton exchange membrane fuel cells, *Electrochim. Acta*, 2013, vol. 92, p. 468.
 28. Zhang, K., Feng, C., He, B., Dong, H., Dai, W., Lu H., and Zhang, X., An advanced electrocatalyst of Pt decorated SnO₂/C nanofibers for oxygen reduction reaction, *J. Electroanal. Chem.*, 2016, vol. 781, p. 198.
 29. Jiang, L., Colmenares, L., Jusys, Z., Sun, G., and Behm, R., Ethanol electrooxidation on novel carbon supported Pt/SnO_x/C catalysts with varied Pt : Sn ratio, *Electrochim. Acta*, 2007, vol. 53, p. 377.
 30. Gharibi, H., Sadeghi, S., and Golmohammadi, F., Electrooxidation of Ethanol on highly active and stable carbon supported PtSnO₂ and its application in passive direct ethanol fuel cell: Effect of tin oxide synthesis method, *Electrochim. Acta*, 2016, vol. 190, p. 1100.
 31. Li, H., Sun, G., Cao, L., Jiang, L., and Xin, Q., Comparison of different promotion effect of PtRu/C and PtSn/C electrocatalysts for ethanol electro-oxidation, *Electrochim. Acta*, 2007, vol. 52, no. 24, p. 6622.
 32. Kim, I., Bong, S., Woo, S., Mahajan, R. K., and Kim, H., Highly active 40 wt % PtRu/C anode electrocatalysts for PEMFCs prepared by an improved impregnation method, *Int. J. Hydrogen Energy*, 2011, vol. 36, no. 2, p. 1803.
 33. Shi, Y., Zhu, W., Shi, H., Liao F., Fan, Z., and Shao, M., Mesocrystal PtRu supported on reduced graphene oxide as catalysts for methanol oxidation reaction, *J. Colloid Interface Sci.*, 2019, vol. 557, p. 729.
 34. Parreira, L.S., da Silva, J.C.M., D’Villa-Silva, M., Simões, F.C., Garcia, S., Gaubeur, I., Cordeiro, M.A.L., Leite, E.R., and dos Santos, M.C., PtSnNi/C nanoparticle electrocatalysts for the ethanol oxidation

- reaction: Ni stability study, *Electrochim. Acta.*, 2013, vol. 96, p. 243.
35. Bonesi, A., Garaventa, G., Triaca, W., and Castroluna, A., Synthesis and characterization of new electrocatalysts for ethanol oxidation *Int. J. Hydrogen Energy*, 2008, vol. 33, № 13, p. 3499.
 36. Parreira, L.S., Antoniassi, R.M., Freitas, I.C., de Oliveira, D.C., Spinacé, E.V., Camargo, P.H.C., and dos Santos, M.C., MWCNT–COOH supported PtSnNi electrocatalysts for direct ethanol fuel cells: Low Pt content, selectivity and chemical stability, *Renewable Energy*, 2019, vol. 143, p. 1397.
 37. Flórez-Montañó, J., García, G., Guillén-Villafuerte, O., Rodríguez, J.L., Planes, G.A., and Pastor, E., Mechanism of ethanol electrooxidation on mesoporous Pt electrode in acidic medium studied by a novel electrochemical mass spectrometry set-up, *Electrochim. Acta*, 2016, vol. 209, p. 121.
 38. Petrii, O.A., The progress in understanding the mechanisms of methanol and formic acid electrooxidation on platinum group metals (a review), *Russ. J. Electrochem.*, 2019, vol. 55, p. 1.
 39. Novomlinskiy, I. N., Guterman, V.E., Danilenko, M.V., and Volochaev, V.A., Platinum Electrocatalysts Deposited onto Composite Carbon Black–Metal Oxide Support, *Russ. J. Electrochem.*, 2019, vol. 55, p. 690.
 40. Zenin, V.V., Spiridonov, B.A., Berezina, N.N., and Kochergin, A.V., Study of electrodeposition and structure of tin–nickel alloy coatings (in Russian), *Tekhnologii v elektron. Promyshlennosti*, 2007, vol. 7, p. 32.
 41. Suryanarayana, C. and Norton, M.G., *X-ray diffraction: a practical approach Suryanarayana C, Springer Sci. Business Media*, 2013, p. 273.
 42. Gražulis, S., Daškevič, A., Merkys, A., Chateigner, D., Lutterotti, L., Quirós, M., Serebryanaya, N.R., Moeck, P., Downs, R.T., and Le Bail, A., Crystallography Open Database (COD): an open-access collection of crystal structures and platform for world-wide collaboration, *Nucleic Acids Res.*, 2012, vol. 40, no. D1, p. 420.
 43. Kirakosyan, S.A., Alekseenko, A.A., Guterman, V.E., Volochaev, V.A., and Tabachkova, N.Y., Effect of CO atmosphere on morphology and electrochemically active surface area in the synthesis of Pt/C and PtAg/C electrocatalysts (in Russian), *Nanotechnologies in Russia*, 2016, vol. 11, p. 287.
 44. Shinozaki, K., Zack, J.W., Pylypenko, S., Pivovar, B.S., and Kocha, S.S., Oxygen Reduction Reaction Measurements on Platinum Electrocatalysts Utilizing Rotating Disk Electrode Technique: II. Influence of Ink Formulation, Catalyst Layer Uniformity and Thickness, *J. Electrochem. Soc.*, 2015, vol. 162, p. 1384.
 45. Kim, J.H., Choi, S.M., Nam, S.H., Seo, M.H., Choi, S.H., and Kim, W.B., Influence of Sn content on PtSn/C catalysts for electrooxidation of C1–C3 alcohols: synthesis, characterization, and electrocatalytic activity, *Appl. Catal. B*, 2008, vol. 82, p. 89.
 46. Colmati, F., Antolini, E., and Gonzalez, E.R., Ethanol oxidation on a carbon-supported Pt₇₅Sn₂₅ electrocatalyst prepared by reduction with formic acid: effect of thermal treatment, *Appl. Catal. B*, 2007, vol. 73, p. 106.
 47. Antolini, E., Salgado, J.R.C., and Gonzalez, E.R., Carbon supported Pt₇₅M₂₅ (M 1/4 Co, Ni) alloys as anode and cathode electrocatalysts for direct methanol fuel cells, *J. Electroanal. Chem.*, 2005, vol. 580, p. 145.
 48. Correa, P.S., da Silva, E.L., da Silva, R.F., Radtke, C., Moreno, B., Chinarro, E., and Malfatti, C.F., Effect of decreasing platinum amount in Pt–Sn–Ni alloys supported on carbon as electrocatalysts for ethanol electrooxidation, *Int. J. Hydrogen Energy*, 2012, vol. 37, no. 11, p. 9314.
 49. Beyhan, S., Léger, J.-M., and Kadırgan, F., Pronounced synergetic effect of the nano-sized PtSnNi/C catalyst for ethanol oxidation in direct ethanol fuel cell, *Appl. Catal. B: Environmental*, 2013, vol. 130, p. 305.
 50. Kumeda, T., Otsuka, N., Tajiri, H., Sakata, O., Hoshi, N., and Nakamura, M., Interfacial structure of PtNi surface alloy on Pt (111) electrode for oxygen reduction reaction, *ACS Omega*, 2017, vol. 2, p. 1858.
 51. Stamenković, V., Schmidt, T.J., Ross, P.N., and Marković, N.M., Surface composition effects in electrocatalysis: kinetics of oxygen reduction on well-defined Pt₃Ni and Pt₃Co alloy surfaces, *J. Phys. Chem.*, 2002, vol. 106, p. 11970.
 52. Jenkins, R. and Snyder, R.L., *Introduction to X-ray Powder Diffractometry*, Wiley, 1996.
 53. Travitsky, N., Ripenbein, T., Golodnitsky, D., Rosenberg, Y., Burshtein, L., and Peled, E., Pt-, PtNi- and PtCo-supported catalysts for oxygen reduction in PEM fuel cells, *J. Power Sources*, 2006, vol. 161, p. 782.
 54. Wiltshire, R.J.K., King, C.R., Rose, A., Wells, P.P., Davies, H., Hogarth, M.P., Thompsett, D., Theobald, B., Mosselmans, F.W., Roberts, M., and Russell, A.E., Effects of composition on structure and activity of PtRu/C catalysts, *Phys. Chem. Chem. Phys.*, 2009, vol. 11, no. 13, p. 2305.
 55. Petrii, O.A., Pt–Ru electrocatalysts for fuel cells: a representative review, *J. Solid State Electrochem.*, 2008, vol. 12, p. 609.
 56. Chen, Y. and Wang, J., Atomic layer deposition assisted Pt–SnO₂ hybrid catalysts on nitrogen-doped CNTs with enhanced electrocatalytic activities for low temperature fuel cells, *Int. J. Hydrogen Energy*, 2011, vol. 36, no. 17, p. 11085.
 57. Ruiz Camacho, B., Morais, C., Valenzuela, M.A., and Alonso-Vante, N., Enhancing oxygen reduction reaction activity and stability of platinum via oxide-carbon composites, *Catal. Today*, 2013, vol. 202, p. 36.
 58. Khorasani-Motlagh, M., Noroozifar, M., and Ekrami-Kakhki, M.-S., Investigation of the nanometals (Ni and Sn) in platinum binary and ternary electrocatalysts for methanol electrooxidation, *Int. J. Hydrogen Energy*, 2011, vol. 36, p. 11554.
 59. Menshchikov, V., Alekseenko, A., Guterman, V., Nechitailov, A., Glebova, N., Tomasov, A., Spiridonova, O., Belenov, S., Zelenina, N., and Safronenko, O., Effective platinum–copper catalysts for methanol oxidation and oxygen reduction in proton-exchange membrane fuel cell, *Nanomaterials*, 2020, vol. 10, no. 4, article No. 742.

Translated by Yu. Pleskov